Available online at www.sciencedirect.com
ScienceDirect
Surface & Coatings Technology 201 (2007) 9256–9259
SURFACE & COATINGS TECHNOLOGY
www.elsevier.com/locate/surfcoat

Chemical routes to ultra thin films for copper barriers and liners

Jinhong Shin [a], Hyun-Woo Kim [b], Gyeong S. Hwang [b], John G. Ekerdt [b,*]

[a] *Materials Science and Engineering, University of Texas at Austin, Austin, TX 78712, USA*
[b] *Department of Chemical Engineering, University of Texas at Austin, Austin, TX 78712, USA*

Available online 23 March 2007

Abstract

Triruthenium dodecarbonyl and trimethylphosphine or triphenylphosphine were used in flowing hydrogen or argon at 575 K to explore the effect of changing the percentage of P on the amorphous character of the films and on the electrical properties of the films. Films as thin as 7 nm were grown. The films contained a carbon impurity that depended on the delivery gas and the alkylphoshphine source. The microstructure changed with the percentage P; amorphous films formed provided the percentage of P exceeded 15 at.%. Film resistivity was most sensitive to the carbon impurity and also changed with microstructure. A 15 nm thick, amorphous film containing ~15 at.% P had a resistivity of 210 μΩ cm. Ion scattering studies reveal that ~0.4 nm Cu films completely wet amorphous Ru–P alloy films. First-principles density-functional calculations are presented revealing the interaction of Ru with P, and predicting that the amorphous structure should be most stable above 20 at.% P.

Keywords: Amorphous; Organometallic CVD; Ruthenium, Phosphorus; *Ab initio* molecular dynamics simulation

1. Introduction

With feature scaling in microelectronic devices, new materials have been adopted, such as Cu for the interconnect wiring. Copper readily diffuses into silicon and through dielectrics and a diffusion barrier is required to prevent this. Copper is also prone to electromigration and seed layer/liner materials that can facilitate both the Cu deposition process and eliminate Cu electromigration are required. The barrier material and the seed layer/liner material combined thickness is projected to be <3.3 nm for the 45-nm generation [1] and a single material that could function as both would be ideal.

Ruthenium shows potential because of its low resistivity of ~7 μΩ cm, chemical stability, low solubility with Cu [2], and ability to form a strong first layer with Cu [3,4]. However, Ru like most metals forms polycrystalline thin films with a columnar character that cannot be expected to function as the Cu diffusion barrier as recently demonstrated [5,6]. Alloying Ru to generate an amorphous film is one approach to enable it to function as both the seed/liner and the diffusion barrier.

We have recently reported the chemical vapor deposition (CVD) growth of amorphous Ru−P alloys containing ~15% P (*n.b.*, compositions on an atom basis) in the bulk using a single source precursor, *cis*-ruthenium(II)dihydrotetrakis-(trimethylphosphine), *cis*-$RuH_2(P(CH_3)_3)$, at 575 K [7,8]. These films were metastable and remained amorphous upon annealing to 635 K for 3 h, and displayed small crystallites in an amorphous matrix upon annealing to 775 K for 1 h [8]. *Ab initio* molecular dynamics calculations [8] revealed that Ru−P alloys with 20% P can result in a glassy structure exhibiting the topological and strong chemical short-range order previously reported for bulk metallic glasses [9–14]. Surface studies revealed the trimethylphosphine ligands of *cis*-$RuH_2(P(CH_3)_3)$ both desorbed intact and underwent a stepwise demethylation to generate the P for Ru−P alloy formation [8].

Herein we report the use of dual sources to explore both how general the Ru−P alloy formation is in CVD and how the P content influences microstructure and resistivity, and we report on gradient corrected density-functional calculations that explore the stability and bonding properties of the amorphous phase. Triruthenium dodecarbonyl, $Ru_3(CO)_{12}$, does not require a reactive gas, like O_2 or H_2 [4,15], and trimethylphosphine, $P(CH_3)_3$, (TMP) is used because surface studies have shown it readily demethylates on Ru to give P by 500 K [16].

* Corresponding author. Tel.: +1 512 471 4689; fax: +1 512 471 7060.
E-mail address: ekerdt@che.utexas.edu (J.G. Ekerdt).

0257-8972/$ - see front matter © 2007 Elsevier B.V. All rights reserved.
doi:10.1016/j.surfcoat.2007.03.019

2. Methods

Film growth was carried out in a deposition and analysis facility consisting of a vacuum sample transfer system, load lock, X-ray photoelectron spectroscopy (XPS) system (Physical Electronics 3057), CVD chamber, and a physical vapor deposition (PVD) chamber [8]. The stainless steel CVD chamber is a cold-wall vessel (base pressure 6.7×10^{-6} Pa) and the SiO_2/Si(100) substrates were heated radiatively from below. Thermally grown SiO_2 (100 nm)/Si(100) 200 mm wafers were supplied by Sematech. The wafers were cut into 20×20 mm pieces and heated to the growth temperature under vacuum. $Ru_3(CO)_{12}$ (Strem Chemical; 99%) was sublimed at 355 K and delivered to the CVD chamber using 2.5−5.0 standard cm^3 per min (sccm) of flowing Ar or H_2 through a heated gas line and shower head. $P(C_6H_5)_3$ (Strem Chemical, 99%) (TPP) was sublimed at 335 K and delivered using 5−10 sccm of flowing Ar through separately heated lines. $P(CH_3)_3$ (Strem Chemical, 99%) was dosed directly into the reaction chamber; the flow was controlled using a leak valve. Crystallinity is established using grazing angle (1°) X-ray diffraction (XRD) (Bruker-Nonius D8). Resistivity was established by measuring the sheet resistance of thin films with a four point probe and the thickness was determined from cross section scanning electron microscopy (SEM) (LEO 1530). Low energy ion scattering spectroscopy (LEISS) was carried out *in situ* using 1 kV He^+. The samples were sputter cleaned with 2 kV Ar^+ before both XPS and LEISS.

Our first principles calculations were performed within the generalized gradient approximation (GGA-PW91 [17]) to density-functional theory (DFT) using the well established Vienna *ab initio* Simulation Package [18,19]. A plane-wave basis set for valence electron states and Vanderbilt ultrasoft pseudopotentials for core–electron interactions were employed. A plane-wave cutoff energy of 300 eV was used and the Brillouin zone integration was performed using one *k*-point (at Gamma). Model amorphous Ru–P alloy structures considered herein were constructed using *ab initio* molecular dynamics within a Born–Oppenheimer framework [7,8].

3. Results and discussion

The effect of growth conditions on the composition and materials properties of the films is summarized in Table 1. The films contain C as an impurity and the exact concentration is difficult to measure. The C 1s and Ru $3d_{3/2}$ XPS peaks at 285 eV overlap and there is no singular unique C peak. Generally one overcomes this overlap by fitting the Ru $3d_{5/2}$ peak and $3d_{3/2}$ peaks, assuming pure Ru has a $3d_{5/2}$ to $3d_{3/2}$ ratio of 1.5 based on the relative degeneracy of the 3d doublet peaks. The Ru 3d peak is 14.4 times mores sensitive than the C 1s peak in XPS [20], so small fitting errors can lead to large concentration errors. On-going experiments are working to quantify the C in the films. The peak ratios are reported in the Table; the ratio decreases as C increases. The films grown with TMP have a lower C content. H_2 was used as the carrier gas to help drive any ligand dehydrogenation reaction in the reverse direction. Films grown with TMP and H_2 show the lowest C. The P content is reported on a C-free basis and the actual P content will be less than the values in Table 1.

In general the microstructure is determined by the P content and ~15% P was necessary for amorphous film growth. This is true for films grown with the dual source reported herein and for films grown with *cis*-$RuH_2(P(CH_3)_3)$ that contained 15% P and had a $3d_{5/2}$ to $3d_{3/2}$ ratio of 1.5 [8]. To confirm this we also calculated total energy differences between crystalline and amorphous Ru–P alloys with varying stoichiometric ratios. As shown in Fig. 1(a), the calculation result also demonstrates that above 20% P the amorphous phase is energetically more favorable than the crystalline phase. Here, the total energy variation of the crystalline alloys was calculated by replacing Ru with P starting with a pure hexagonal close packed Ru phase, which is modeled using a 72-atom supercell with a lattice constant of 2.70 Å. For each crystalline or amorphous alloy considered, the volume of the 72-atom supercell was optimized by determining the minimum total energy with varying supercell volumes. As shown in Fig. 1(b), the alloy volume becomes the minimum at 20% P, yielding the highest packing density.

Fig. 2 shows a variation in the mixing energy of amorphous Ru–P alloys as a function of the stoichiometric ratio, with respect to amorphous Ru and P. The negative mixing energy demonstrates that the alloy state is thermodynamically favored in the amorphous phase. Our density-functional calculations also predict that the Ru–P alloy forms the most stable structure when the P content is around 40–50%. The sizable energy gain of the $Ru_{60}P_{40}$ structure, relative to the $Ru_{80}P_{20}$ structure, suggests that the Ru–P alloys with a low P content (~20%) may

Table 1
Effect of phosphorus and carbon content on the film microstructure and resistivity

Sample	Phosphorus source	Delivery gas	Thickness (nm)	Ru $3d_{5/2}$ to $3d_{3/2}$ ratio	P/(P+Ru) (at.%)	Resistivity (μΩ cm)	Microstructure
1	TPP[a]	Ar	39	1.18	12.0	12,624	Crystalline
2	TPP	Ar	33	1.03	19.6	1,099,506	Amorphous
3	TMP[b]	Ar	61	1.32	5.2	263	Crystalline
4	TMP	Ar	11	1.22	20.0	864	Amorphous
5	TMP	H_2	17	1.45	8.5	59	Crystalline
6	TMP	H_2	15	1.38	15.3	209	Amorphous
7	TMP	H_2	<10	1.31	26.9	367	Amorphous

[a] Triphenylphosphine.
[b] Trimethylphosphine.

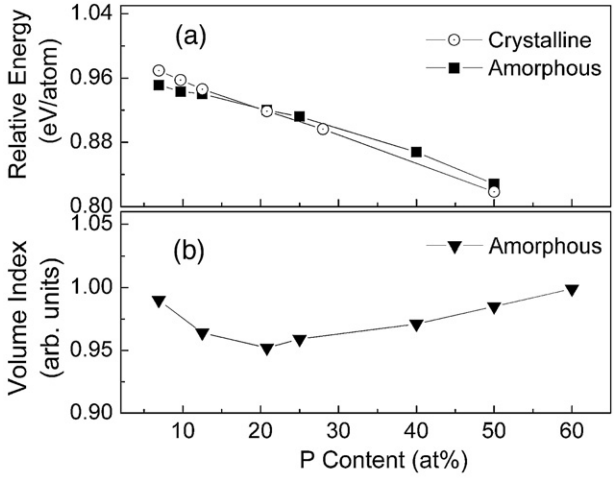

Fig. 1. Variation in (a) the total energy difference between the crystalline and amorphous phases and (b) the optimized volume of Ru–P alloys as a function of the P content.

undergo P segregation during high temperature thermal treatment.

To gain understanding of the Ru–P bonding properties, as shown in Fig. 3 we analyzed the density of states (DOS) of the $Ru_{80}P_{20}$ alloy (inset), including the total DOS [(a)] and the partial DOS of Ru 4d [(b)] and P 3p [(c)]. The Fermi level is used as the reference energy state. The calculated total DOS shows no gap at the Fermi level, indicating that the Ru–P alloy is metallic. In Fig. 3(a), peaks below −10 eV are assigned to the P 3s state, and the peaks of occupied state densities above −10 eV mainly originate from the P 3p and Ru 4d orbitals. In the energy range between −4 and −7, we can see a high degree of hybridization of Ru 3d with P 3p states. It is apparent that the p–d hybridization mainly contributes to stabilizing the Ru–P alloy structure.

The seed layer for Cu plating needs to have as low a resistivity as possible; bulk Ru has a resistivity of ~7 μΩ cm, which makes it a viable seed layer material. The results in Table 1 illustrate that resistivity is most sensitive to the C content of the films, as reflected in the Ru 3d peak ratios, increasing with C content. Microstructure is also a factor since

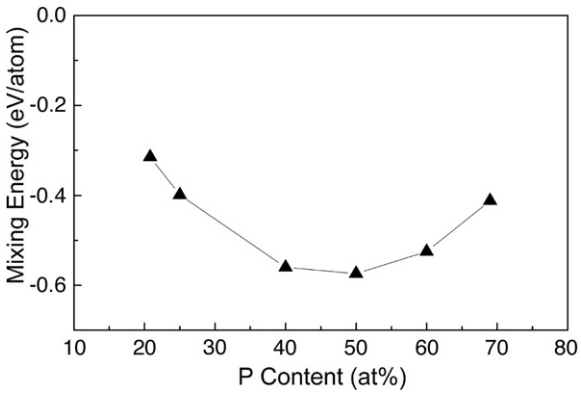

Fig. 2. Variation of the mixing energy of amorphous Ru–P alloys in terms of the P content, with respective to amorphous Ru and P structures.

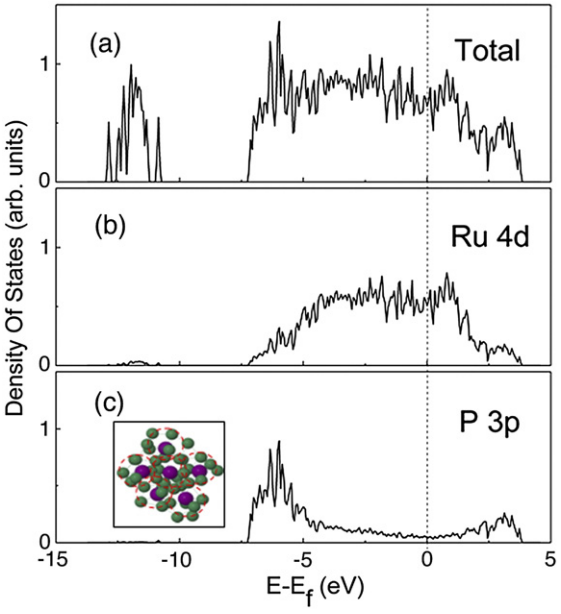

Fig. 3. Calculated densities of states (DOS) for the $Ru_{80}P_{20}$ alloy, as shown in inset (c): (a) total, (b) Ru 4d, and (c) P 3p. The Fermi level is indicated as a dotted line.

films of comparable C content (Samples 3 and 7) illustrate that crystalline films will have a lower resistivity.

Previous studies have revealed that CVD Ru growth on SiO_2 from $Ru_3(CO)_{12}$ resulted in polycrystalline films having a columnar structure, due to the high surface energy of Ru (3.05 J/m^2 for Ru(0001)). The study also showed that a film greater than 20 nm was needed to fully cover the SiO_2 surface [15]. Herein we show that amorphous Ru(P) films as thin as 7.1 nm are continuous (Fig. 4). This is established using XPS to follow the intensity changes in the substrate peaks as the Ru(P) films

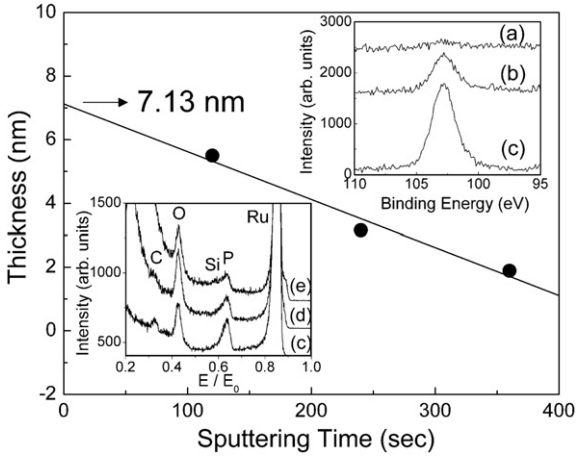

Fig. 4. Thickness of a Ru(P) film deposited on SiO_2 that was determined by sputtering the film with Ar^+ and monitoring the escape of Si 2p XPS peak intensity. The inset (top right) shows the Si 2p peak intensity after sputtering for (a) 120 s, (b) 240 s, and (c) 360 s with 2 kV Ar^+. The points were determined using an electron inelastic mean free path of 1.671 nm. The inset (bottom left) shows the LEISS data after sputtering for (c) 360 s, (d) 480 s, and (e) 600 s with 2 kV Ar^+. The Si feature becomes discernable after 600 s of sputtering, indicating the underlying SiO_2 substrate has been reached.

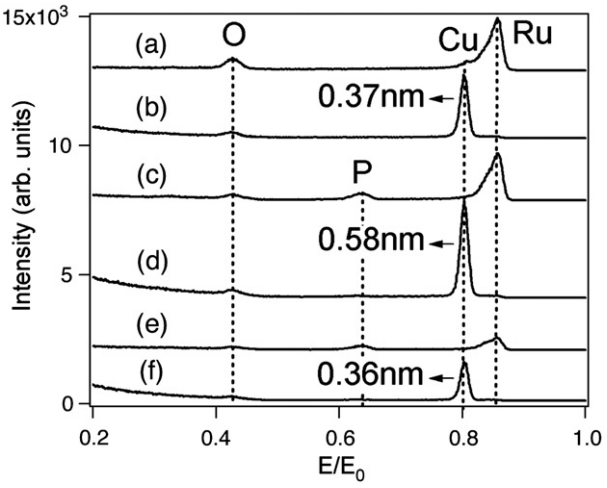

Fig. 5. LEISS results showing the wettability of Cu on Ru and Ru(P) films. (a) PVD Ru film, (b) 0.37 nm PVD Cu on the PVD Ru film, (c) CVD Ru(P) film grown from $Ru_3(CO)_{12}$ and $P(CH_3)_3$ containing 14.9% P and with a Ru $3d_{5/2}$ to $3d_{3/2}$ ratio of 1.39, (d) 0.58 nm PVD Cu on the CVD Ru(P) film grown from $Ru_3(CO)_{12}$ and $P(CH_3)_3$, (e) CVD Ru(P) film grown with *cis*-$RuH_2(P(CH_3)_3)_4$ containing 28.1% P and with a Ru $3d_{5/2}$ to $3d_{3/2}$ ratio of 1.38, and (f) 0.36 nm CVD Cu on the CVD Ru(P) film grown with *cis*-$RuH_2(P(CH_3)_3)_4$.

becomes thinned with Ar^+ sputtering and LEISS to monitor the composition of the top most layer. The inelastic mean free path of Si 2p electrons through Ru is used to compute film thickness assuming a uniform and flat film. The lower minimum thickness for continuous amorphous Ru(P) films compared to polycrystalline Ru films can be attributed to the lower nucleation energy of the amorphous phase and better wettability because incorporation of P and C lower the surface energy [21].

Strong copper adhesion to the liner material (*i.e.*, diffusion barrier and seed layer(s)) is one metric that is necessary to minimize copper electromigration in copper interconnect applications [22]. Fig. 5 presents the LEISS results for two different CVD films that contain different amounts of P and C. The conditions used to grow the film with *cis*-$RuH_2(P(CH_3)_3)_4$ are found elsewhere [7,8]. The Cu is deposited using PVD and the total time is 5 s, making it difficult to realize thinner films. Cu film thickness is established using attenuation of the Ru $3d_{5/2}$ XPS peak and assumes the Cu film is uniform. The LIESS data (Fig. 5) demonstrate that films as thin as 0.4–0.6 nm completely wet the Ru(P) films, and that the presence of P up to ~30% at the surface does not lead to Cu dewetting and forming islands.

4. Conclusions

Chemical vapor deposition growth of amorphous ruthenium–phosphorus films on SiO_2 is demonstrated at 575 K provided the P content is greater than 15%. First-principles density-functional calculations are presented revealing the interaction of Ru with P, and predicting that the amorphous structure should be most stable above 20 at.% P.

Acknowledgments

This work was supported by the Semiconductor Research Corporation (Contract 2006-KC-1292.016) and the National Science Foundation (Grant CTS-0553839).

References

[1] International Technology Roadmap for Semiconductors, 2006 Updated ed, 2007. Available at <http://public/itrs.net>.
[2] I. Goswami, R. Laxman, Semicond. Int. 27 (2004) 49.
[3] J.E. Houston, P.J. Berlowitz, J.M. White, D.W. Goodman, J. Vac. Sci. Technol. A 6 (1988) 887.
[4] Q. Wang, J.G. Ekerdt, D. Gay, Y. Sun, J.M. White, Appl. Phys. Lett. 84 (2004) 1380.
[5] R. Chan, T.N. Arunagiri, Y. Zhang, O. Chyan, R.M. Wallace, M.J. Kim, T.Q. Hurd, Electrochem. Solid-State Lett. 7 (2004) G154.
[6] J. Tan, X. Qu, Q. Xie, Y. Zhou, G. Ru, Thin Solid Films 504 (2006) 231.
[7] J-H. Shin, A. Waheed, K. Agapiou, W.A. Winkenwerder, H-W. Kim, R.A. Jones, G.S. Hwang, J.G. Ekerdt, J. Am. Chem. Soc. 128 (2006) 16510.
[8] J-H. Shin, A. Waheed, W.A. Winkenwerder, H-W. Kim, K. Agapiou, R.A. Jones, G.S. Hwang, J.G. Ekerdt, Thin Solid Films 515 (2007) 5298.
[9] O.N. Senkov, D.B. Miracle, Mater. Res. Bull. 36 (2001) 2183.
[10] R. Busch, J. Mater. 52 (2000) 39.
[11] J. Basu, S. Ranganathan, Sadhana 28, Parts 3 & 4 (2003) 783.
[12] L. Xia, S.S. Fang, Q. Wang, Y.D. Dong, C.T. Liu, Appl. Phys. Lett. 88 (2006) 171905.
[13] H.-J. Lee, T. Cagin, W.L. Johnson, W.A. Goddard III, J. Chem. Phys. 119 (2003) 9858.
[14] H.W. Sheng, W.K. Luo, F.M. Alamgir, J.M. Bai, E. Ma, Nature 439 (2006) 419.
[15] J. Shin, D. Gay, Y-M. Sun, J.M. White, J.G. Ekerdt, in: D.G. Seiler, A.C. Diebold, R. McDonald, C.R. Ayre, R.P. Khosla, S. Zollner, E.M. Secula (Eds.), AIP Conf. Proc., vol. 788, Melville, NY, 2005, p. 482.
[16] H.-S. Tao, U. Diebold, N.D. Shinn, T.E. Madey, Surf. Sci. 375 (1997) 257.
[17] J.P. Perdew, J.A. Chevary, S.H. Vosko, K.A. Jackson, M.R. Pederson, D.J. Singh, C. Fiolhais, Phys. Rev., B 46 (1992) 6671.
[18] G. Kresse, J. Hafner, Phys. Rev., B 47 (1993) 553.
[19] G. Kresse, J. Furthmüller, Phys. Rev., B 54 (1996) 11169.
[20] D. Briggs, M.P. Seah, Practical Surface Analysis. vol 1. Auger and X-ray Photoelectron Spectroscopy, John Wiley and Sons, Chichester, 1990, p. 635.
[21] K.N. Tu, J.W. Mayer, L.C. Feldman, Electronic Thin Film Science, Mcmillian, New York, 1992, p. 246.
[22] H. Kim, Y. Naito, T. Koseki, T. Ohba, T. Ohta, Y. Kojima, H. Sato, Y. Shimogaki, Jpn. J. Appl. Phys. 45 (2006) 2497.